JOC Article

pubs.acs.org/joc

Stapling of a 3_{10}-Helix with Click Chemistry

Øyvind Jacobsen,*,† Hiroaki Maekawa,‡ Nien-Hui Ge,‡ Carl Henrik Görbitz,§ Pål Rongved,† Ole Petter Ottersen,¶ Mahmood Amiry-Moghaddam,¶ and Jo Klaveness†

†School of Pharmacy, University of Oslo, P.O. Box 1068 Blindern, 0316 Oslo, Norway, ‡Department of Chemistry, University of California at Irvine, Irvine, California 92697-2025, United States, §Department of Chemistry, University of Oslo, P.O. Box 1033 Blindern, 0315 Oslo, Norway, and ¶Centre for Molecular Biology and Neuroscience, University of Oslo, P.O. Box 1105 Blindern, 0317 Oslo, Norway

oyvind.jacobsen@farmasi.uio.no

Received August 25, 2010

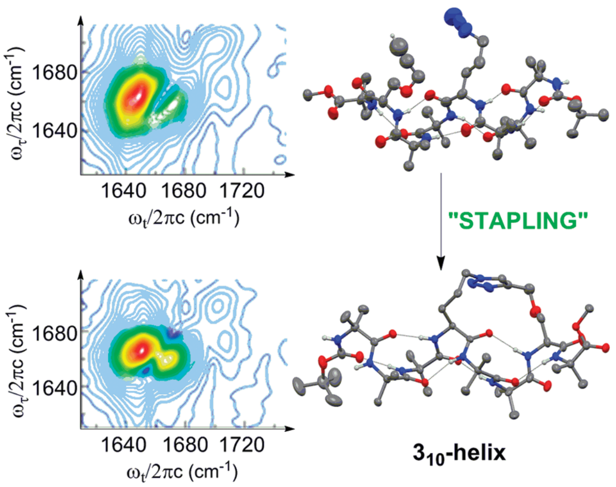

Short peptides are important as lead compounds and molecular probes in drug discovery and chemical biology, but their well-known drawbacks, such as high conformational flexibility, protease lability, poor bioavailability and short half-lives *in vivo*, have prevented their potential from being fully realized. Side chain-to-side chain cyclization, e.g., by ring-closing olefin metathesis, known as stapling, is one approach to increase the biological activity of short peptides that has shown promise when applied to 3_{10}- and α-helical peptides. However, atomic resolution structural information on the effect of side chain-to-side chain cyclization in 3_{10}-helical peptides is scarce, and reported data suggest that there is significant potential for improvement of existing methodologies. Here, we report a novel stapling methodology for 3_{10}-helical peptides using the copper(I)-catalyzed azide−alkyne cycloaddition (CuAAC) reaction in a model aminoisobutyric acid (Aib) rich peptide and examine the structural effect of side chain-to-side chain cyclization by NMR, X-ray diffraction, linear IR and femtosecond 2D IR spectroscopy. Our data show that the resulting cyclic peptide represents a more ideal 3_{10}-helix than its acyclic precursor and other stapled 3_{10}-helical peptides reported to date. Side chain-to-side chain stapling by CuAAC should prove useful when applied to 3_{10}-helical peptides and protein segments of interest in biomedicine.

Introduction

The concept of introducing conformational constraints in peptides that stabilize their biologically active secondary structure has attracted a lot of interest as a way to improve the pharmacological properties of peptides. In particular, this concept has been successfully applied to α-helical peptides and protein segments. Examples include peptides with intramolecular H-bond surrogates[1] and so-called stapled

(1) Vernall, A. J.; Cassidy, P.; Alewood, P. F. *Angew. Chem., Int. Ed.* **2009**, *48*, 5675.

Published on Web 01/28/2011 DOI: 10.1021/jo101670a

peptides, the latter deriving helix stabilization from side chain-to-side chain hydrophobic interactions,[2] salt bridges,[3] disulfide bridges,[4] lactams,[5] and metathesis derived hydrocarbon bridges.[6−8] Significantly, hydrocarbon stapling of α-helical peptides has afforded several compounds that could have clinical potential, e.g., against cancer.[9−11] The structural and pharmacological effects of ring-closing metathesis in peptides have recently been reviewed.[12] Recently, hydrocarbon stapling has also been successfully applied to 3_{14}-helical β-peptides,[13] extending its range of applicability beyond α-peptides.

The 3_{10}-helix, which is defined by intramolecular $i \rightarrow i+3$ H-bonds, is an important structural element in proteins, peptide antibiotics known as peptaibols,[14] and many biological recognition processes, as well as a postulated intermediate structure in protein folding.[15]

Over the past decade the predominant water channel in the mammalian brain, aquaporin-4 (AQP4), has emerged as an important target for treatment of brain edema after stroke or trauma.[16−19] As part of an ongoing project to design selective inhibitors of AQP4 we have been interested in side chain-to-side chain bridges that allow some stabilization of the 3_{10}-helical conformation of the Pro138-Gly144 segment of human AQP4,[20] which has been postulated to mediate adhesive interactions between two AQP4 tetramers.[21−23]

Examples of $i \rightarrow i+3$ and $i \rightarrow i+4$ side chain-to-side chain cross-linking in 3_{10}-helical peptides by Glu-Lys lactam formation,[24] ferrocenedicarboxylic acid Lys diamides,[25] photoinduced 1,3-dipolar cycloaddition,[26] metathesis derived hydrocarbon bridges,[20,27,28] and a *p*-phenylenediacetic acid bridge[29] between two α,α-disubstituted 4-aminopiperidine-4-carboxylic acid (Api) residues have been reported. However, only two studies[28,29] have provided atomic resolution detail of the effect of cyclization on helix regularity, i.e., on backbone dihedral angles and H-bond lengths.

In the first X-ray crystallographic study[28] of the effect of side chain-to-side chain cyclization in a 3_{10}-helical peptide it was observed that the backbone is distorted by an $i \rightarrow i+3$ metathesis derived olefinic bridge, resulting in the breakage of one intramolecular H-bond, thus disrupting the 3_{10}-helix. The *p*-phenylenediacetic acid bridge on the other hand appears to afford a highly regular Api/Aib based 3_{10}-helix.[29] However, α,α-disubstituted amino acids such as Aib and *N*-acylated Api are generally hydrophobic and tend to distort the dihedral angles of neighboring monosubstituted, proteinogenic residues away from ideality.[24,28,30] In the context of a helical peptide primarily consisting of proteinogenic amino acids, *mono*substituted residues are expected to be better tolerated. Hence, new methodology for cross-linking of monosubstituted residues, which does not significantly distort the regularity of the 3_{10}-helix, is highly desirable. If, at the same time, the cross-linking results in a more hydrophilic bridge, thus increasing the aqueous solubility of the stapled peptide, such a methodology could potentially have broad utility. In particular, the resulting stapled peptides should be useful for the study and modulation of biologically important recognition processes involving 3_{10}-helical peptides and protein segments.

There has been an explosion of interest in click chemistry[31] in recent years, exemplified by the highly popular copper(I)-catalyzed azide−alkyne cycloaddition (CuAAC) reaction.[32−35] This reaction has been successfully applied to $i \rightarrow i+4$ side chain-to-side chain cyclization in an α-helical peptide[36,37] and $i \rightarrow i+3$ cyclization in peptoids (peptides composed of *N*-substituted glycines).[38] The high functional group tolerance of the CuAAC reaction, the very large dipole moment

(2) Munoz, V.; Blanco, F. J.; Serrano, L. *Nat. Struct. Biol.* **1995**, *2*, 380.
(3) Scholtz, J. M.; Qian, H.; Robbins, V. H.; Baldwin, R. L. *Biochemistry* **1993**, *32*, 9668 and references therein.
(4) Jackson, D. Y.; King, D. S.; Chmielewski, J.; Singh, S.; Schultz, P. G. *J. Am. Chem. Soc.* **1991**, *113*, 9391.
(5) Phelan, J. C.; Skelton, N. J.; Braisted, A. C.; McDowell, R. S. *J. Am. Chem. Soc.* **1997**, *119*, 455 and references therein.
(6) Blackwell, H. E.; Grubbs, R. H. *Angew. Chem., Int. Ed.* **1998**, *37*, 3281.
(7) Schafmeister, C. E.; Po, J.; Verdine, G. L. *J. Am. Chem. Soc.* **2000**, *122*, 5891.
(8) Young-Woo, K.; Verdine, G. L. *Bioorg. Med. Chem. Lett.* **2009**, *19*, 2533.
(9) Walensky, L. D.; Kung, A. L.; Escher, I.; Malia, T. J.; Barbuto, S.; Wright, R. D.; Wagner, G.; Verdine, G. L.; Korsmeyer, S. J. *Science* **2004**, *305*, 1466.
(10) Moellering, R. E.; Cornejo, M.; Davis, T. N.; Del Bianco, C.; Aster, J. C.; Blacklow, S. C.; Kung, A. L.; Gilliland, D. G.; Verdine, G. L.; Bradner, J. E. *Nature* **2009**, *462*, 182.
(11) Gavathiotis, E.; Suzuki, M.; Davis, M. L.; Pitter, K.; Bird, G. H.; Katz, S. G.; Tu, H.-C.; Kim, H.; Cheng, E. H.-Y.; Tjandra, N.; Walensky, L. D. *Nature* **2008**, *455*, 1076.
(12) Jacobsen, Ø.; Klaveness, J.; Rongved, P. *Molecules* **2010**, *15*, 6638.
(13) Ebert, M.-O.; Gardiner, J.; Ballet, S.; Abell, A. D.; Seebach, D. *Helv. Chim. Acta* **2009**, *92*, 2643.
(14) *Peptaibiotics: Fungal Peptides Containing α-Dialkyl α-Amino Acids*; Toniolo, C., Brückner, H., Eds.; Wiley-VCH: New York, 2009.
(15) Millhauser, G. L. *Biochemistry* **1995**, *34*, 3873.
(16) Manley, G. T.; Fujimura, M.; Ma, T.; Noshita, N.; Fliz, F.; Bollen, A. W.; Chan, P.; Verkman, A. S. *Nat. Med.* (*N. Y.*) **2000**, *6*, 159.
(17) Vajda, Z.; Pedersen, M.; Fuchtbauer, E.-M.; Wertz, K.; Stodkilde-Jorgensen, H.; Sulyok, E.; Doczi, T.; Neely, J. D.; Agre, P.; Frokiaer, J.; Nielsen, S. *Proc. Natl. Acad. Sci. U.S.A.* **2002**, *99*, 13131.
(18) Amiry-Moghaddam, M. R.; Otsuka, T.; Hurn, P. D.; Traystman, R. J.; Haug, F. M.; Stanley, S. C.; Adams, M. E.; Neely, J. D.; Agre, P.; Ottersen, O. P.; Bhardwaj, A. *Proc. Natl. Acad. Sci. U.S.A.* **2003**, *100*, 2106.
(19) Amiry-Moghaddam, M.; Ottersen, O. P. *Nat. Rev. Neurosci.* **2003**, *4*, 991.
(20) Jacobsen, Ø.; Klaveness, J.; Ottersen, O. P.; Amiry-Moghaddam, M. R.; Rongved, P. *Org. Biomol. Chem.* **2009**, *7*, 1599.
(21) Tani, K.; Mitsuma, T.; Hiroaki, Y.; Kamegawa, A.; Nishikawa, K.; Tanimura, Y.; Fujiyoshi, Y. *J. Mol. Biol.* **2009**, *389*, 694.
(22) Engel, A.; Fujiyoshi, Y. *Curr. Opin. Struct. Biol.* **2008**, *18*, 229.
(23) Hiroaki, Y.; Tani, K.; Kamegawa, A.; Gyobu, N.; Nishikawa, K.; Suzuki, H.; Walz, T.; Sasaki, S.; Mitsuoka, K.; Kimura, K.; Mizoguchi, A.; Fujiyoshi, Y. *J. Mol. Biol.* **2006**, *355*, 628.
(24) Schievano, E.; Pagano, K.; Mammi, S.; Peggion, E. *Biopolymers* **2005**, *80*, 294.
(25) Curran, T. P.; Handy, E. L. *J. Organomet. Chem.* **2009**, *694*, 902.
(26) Madden, M. M.; Rivera Vera, C. I.; Song, W.; Lin, Q. *Chem. Commun.* **2009**, No. 37, 5588.
(27) Blackwell, H. E.; Sadowsky, J. D.; Howard, R. J.; Sampson, J. N.; Chao, J. A.; Steinmetz, W. E.; O'Leary, D. J.; Grubbs, R. H. *J. Org. Chem.* **2001**, *66*, 5291.
(28) Boal, A. K.; Guryanov, I.; Moretto, A.; Crisma, M.; Lanni, E. L.; Toniolo, C.; Grubbs, R. H.; O'Leary, D. J. *J. Am. Chem. Soc.* **2007**, *129*, 6986.
(29) Ousaka, N.; Sato, T.; Kuroda, R. *J. Am. Chem. Soc.* **2008**, *130*, 463.
(30) Bavoso, A.; Benedetti, E.; Di Blasio, B.; Pavone, V.; Pedone, C.; Toniolo, C.; Bonora, G. M. *Proc. Natl. Acad. Sci. U.S.A.* **1986**, *83*, 1988.
(31) Kolb, H. C.; Finn, M. G.; Sharpless, K. B. *Angew. Chem., Int. Ed.* **2001**, *40*, 2004.
(32) Tornøe, C. W.; Meldal, M. *Peptides 2001, Proceedings of the American Peptide Symposium*; American Peptide Society and Kluwer Academic Publishers: San Diego, 2001; pp 263−264.
(33) Tornøe, C. W.; Christensen, C.; Meldal, M. *J. Org. Chem.* **2002**, *67*, 3057.
(34) Rostovtsev, V. V.; Green, L. G.; Fokin, V. V.; Sharpless, B. K. *Angew. Chem., Int. Ed.* **2002**, *41*, 2596.
(35) Meldal, M.; Tornøe, C. W. *Chem. Rev.* **2008**, *108*, 2952.
(36) Cantel, S.; Le Chevalier Isaad, A.; Scrima, M.; Levy, J. J.; DiMarchi, R. D.; Rovero, P.; Halperin, J. A.; D'Ursi, A. M.; Papini, A. M.; Chorev, M. *J. Org. Chem.* **2008**, *73*, 5663.
(37) Scrima, M.; Le Chevalier-Isaad, A.; Rovero, P.; Papini, A. M.; Chorev, M.; D'Ursi, A. M. *Eur. J. Org. Chem.* **2010**, No. 3, 446.
(38) Holub, J. M.; Jang, H.; Kirshenbaum, K. *Org. Lett.* **2007**, *9*, 3275.

SCHEME 1. Final Steps of the Synthesis of the Acyclic Peptide 1

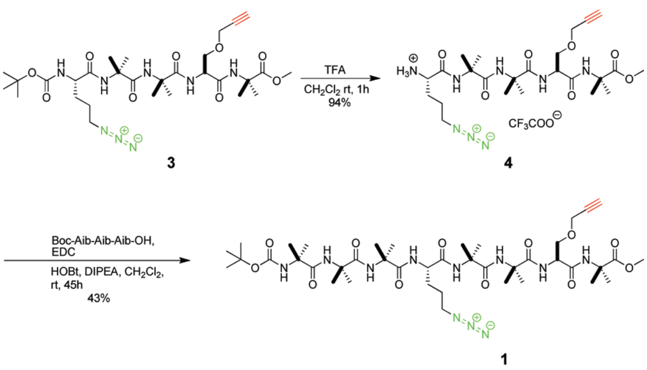

SCHEME 2. Final Steps of the Synthesis of the Cyclic Peptide 2

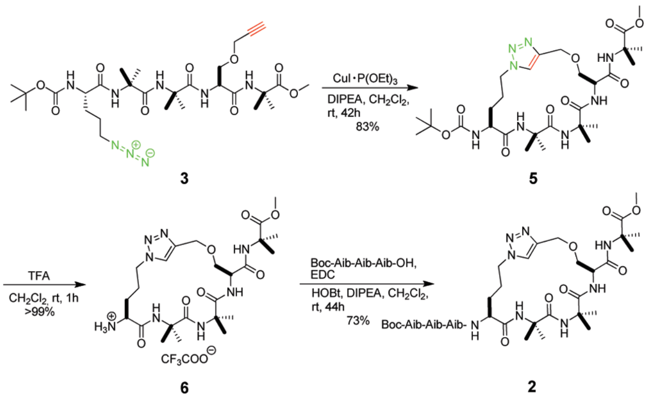

(~5 D)[39] and the relatively high resistance to metabolic degradation[40,41] of the 1,2,3-triazole moiety make 3_{10}-helical peptides with a side chain-to-side chain triazole bridge highly interesting objects of study.

In this paper we report the installation of an $i \rightarrow i+3$ constraint by side chain-to-side chain CuAAC between two monosubstituted residues in the context of a 3_{10}-helical Aib rich peptide and examine in detail the effect of cyclization on helix regularity by X-ray crystallography, NMR, linear IR and 2D IR spectroscopy. To allow a direct comparison with the results for the $i \rightarrow i+3$ hydrocarbon bridge, two octapeptides **1** (Scheme 1) and **2** (Scheme 2) with the reactive/cross-linked residues in the same Aib rich context as the olefinic peptides of Boal et al.[28] were chosen as synthetic targets.

To the best of our knowledge, this study represents the first X-ray structural investigation of a (α- or 3_{10}-) helical peptide after stapling by CuAAC or with a triazole derived conformational constraint and the first 2D IR structural investigation of a 3_{10}-helical peptide with a conformational constraint installed. Given the widespread interest in the CuAAC reaction, it is important to note that this study also affords what appears to be the first crystal structure of a bifunctional azide−alkyne compound.

(39) Bourne, Y.; Kolb, H. C.; Radic, Z.; Sharpless, K. B.; Taylor, P.; Marchot, P. *Proc. Natl. Acad. Sci. U.S.A.* **2004**, *101*, 1449.

(40) Whiting, M.; Muldoon, J.; Lin, Y. C.; Silverman, S. M.; Lindstrom, W.; Olson, A. J.; Kolb, H. C.; Finn, M. G.; Sharpless, K. B.; Elder, J. H.; Fokin, V. V. *Angew. Chem., Int. Ed.* **2006**, *45*, 1435.

(41) Tornøe, C. W.; Sanderson, S. J.; Mottram, J. C.; Coombs, G. H.; Meldal, M. *J. Comb. Chem.* **2004**, *6*, 312.

Results and Discussion

Peptide Synthesis. The building block N^{α}-Boc-δ-azido-L-norvaline[42] was synthesized in 63% yield from N^{α}-Boc-L-ornithine using a recently developed shelf-stable and crystalline diazo transfer reagent, imidazole-1-sulfonyl azide hydrochloride.[43] *N*-Boc-*O*-propynyl-L-serine[44] was synthesized in 77% yield by a variation of Sugano's method for synthesis of *N*-Boc-*O*-benzyl-L-serine.[45] The octapeptide **1** was assembled by a segment condensation strategy using standard solution phase peptide coupling chemistry employing EDC/HOBt in DMF or CH_2Cl_2 (Supporting Information). The final steps involved deprotection of pentapeptide **3** with TFA/CH_2Cl_2 (1:1(v/v)) and coupling of the resulting trifluoroacetate **4** with Boc-Aib-Aib-Aib-OH[28] to afford the octapeptide **1** in 43% yield (Scheme 1).

A recent investigation of Aib oligopeptides by 2D IR spectroscopy revealed that the onset of 3_{10}-helical structure appears to occur already at the pentapeptide level in $CDCl_3$.[46] This, together with our previous success in cyclizing an olefinic pentapeptide by ring-closing metathesis[20] in CH_2Cl_2 suggested that cyclization by CuAAC might be possible at the pentapeptide level in CH_2Cl_2. At high dilution (~0.15 mM) **3** was cyclized to **5** in 83% yield (Scheme 2) in the presence of 0.31 equiv of the organic-soluble copper(I) complex CuI·P(OEt)$_3$, which was synthesized according to a literature procedure.[47,48] Dimerization and cyclodimerization are competing processes and have resulted in relatively low yields of cyclic monomer in several instances of intramolecular CuAACs, even at high dilution.[35,49,50] The relatively high yield in this case suggests a high degree of substrate preorganization in CH_2Cl_2. Deprotection of **5** with TFA/CH_2Cl_2 (1:1(v/v)), yielding the trifluoroacetate **6**, followed by segment condensation with Boc-Aib-Aib-Aib-OH[28] afforded octapeptide **2** in 73% yield over two steps (Scheme 2). This synthesis strategy for the synthesis of **2** has the advantage over direct cyclization of **1** that it allows the most challenging synthetic step, namely, the macrocyclization, to be carried out at the earliest possible stage. Later structural studies (below) demonstrated that **1** is predominantly 3_{10}-helical in CH_2Cl_2 solution, suggesting that cyclization would have been successful also at the octapeptide level. However, the yield obtained on cyclization of **3** was considered satisfactory and rendered the alternative strategy superfluous and untested in this particular study.

X-ray Crystallography. Peptide **1** ($C_{41}H_{69}N_{11}O_{12}$, M_w = 908.05) (Scheme 1) crystallized as colorless, plate-shaped crystals in space group $P2_12_12_1$, with unit cell parameters a = 16.239(12), b = 18.236(14), c = 18.655(14) Å, α = 90.00°, β = 90.00°, γ = 90.00° (orthorhombic crystal system) and Z = 4. The X-ray structure was refined to a final *R*-factor of 0.068 for

(42) Le Chevalier Isaad, A.; Barbetti, F.; Rovero, P.; D'Ursi, A. M.; Chelli, M.; Chorev, M.; Papini, A. M. *Eur. J. Org. Chem.* **2008**, No. 31, 5308.

(43) Goddard-Borger, E. D.; Stick, R. V. *Org. Lett.* **2007**, *9*, 3797.

(44) ten Brink, H. T.; Rijkers, D. T. S.; Liskamp, R. M. J. *J. Org. Chem.* **2006**, *71*, 1817.

(45) Sugano, H.; Miyoshi, M. *J. Org. Chem.* **1976**, *41*, 2352.

(46) Maekawa, H.; Formaggio, F.; Toniolo, C.; Ge, N.-H. *J. Am. Chem. Soc.* **2008**, *130*, 6556.

(47) Langille, N. F.; Jamison, T. F. *Org. Lett.* **2006**, *8*, 3761.

(48) Nishizawa, Y. *Bull. Chem. Soc. Jpn.* **1961**, *34*, 1170.

(49) Jagasia, R.; Holub, J. M.; Bollinger, M.; Kirshenbaum, M.; Finn, M. G. *J. Org. Chem.* **2009**, *74*, 2964.

(50) Angell, Y.; Burgess, K. *J. Org. Chem.* **2005**, *70*, 9595.

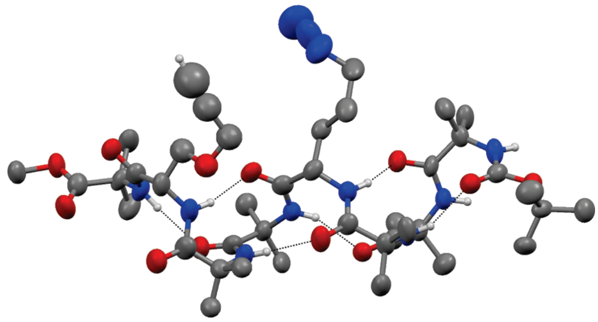

FIGURE 1. Thermal ellipsoid plot of the X-ray crystal structure of the acyclic peptide **1** at the 50% probability level with intramolecular H-bonds indicated. Apolar hydrogens have been omitted for clarity. The major backbone conformation at Aib6 is shown (see Supporting Information for details).

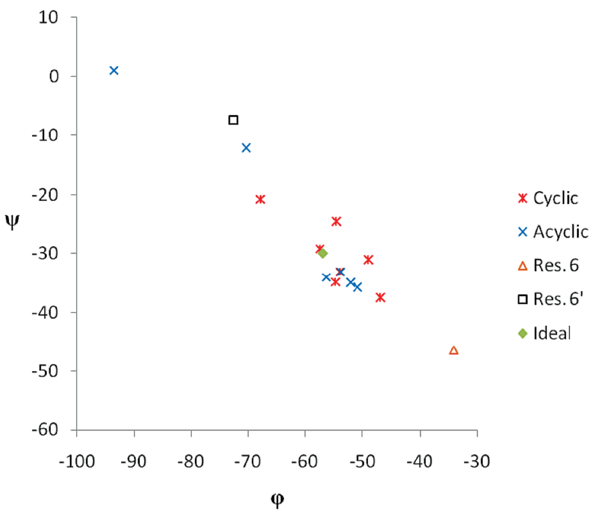

FIGURE 2. Partial Ramachandran plot for residues 1−7 of **1** and **2**. Both conformations of Aib6 in the crystal structure of **1** are indicated (Res. 6: major conformation; Res. 6′: minor conformation). See Supporting Information for details and complete Ramachandran plots.

data obtained for a very small crystal (0.100 mm × 0.010 mm × 0.009 mm). The peptide forms a fully developed right handed 3_{10}-helix with all possible intramolecular $i \rightarrow i+3$ H-bonds present, including between the *tert*-butoxycarbonyl (Boc) group and the amide NH of Aib3 (Figure 1).

With the exceptions of residues 4, 6, 7, and 8 the conformations of all remaining residues fall into the 3_{10}-helical region of (φ, ψ)-space, with the mean absolute deviations from the ideal (i.e., average observed in peptides) 3_{10}-helical angles of (−57°, −30°)[51] being 3.68° and 4.48°, respectively (Figure 2).

However, the dihedral angles of the two chiral, monosubstituted residues 4 and 7 deviate significantly from the ideal 3_{10}-helical angles, with $[(|\Delta\varphi|, |\Delta\psi|) = (13.38°, 17.90°)$ and $(36.55°, 30.96°)]$ respectively. Similarly large deviations from ideality, albeit slightly smaller for residue 4, were observed for the acyclic olefinic peptide of Boal et al.[28] Here, residue 7, for which $(\varphi, \psi)_7 = (-93.55°, 0.96°)$, forms part of a type-I

(51) Toniolo, C.; Benedetti, E. *Trends Biochem. Sci.* **1991**, *16*, 350.
(52) Chou, P. Y.; Fasman, G. D. *J. Mol. Biol.* **1977**, *115*, 135.
(53) Venkatachalam, C. M. *Biopolymers* **1968**, *6*, 1425.

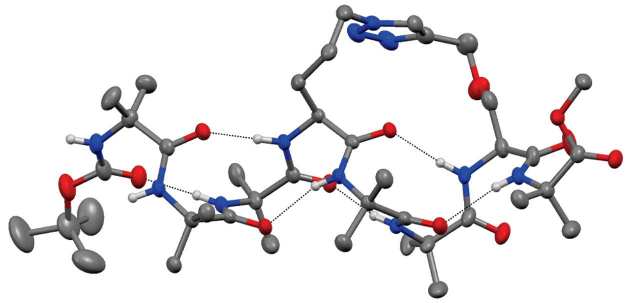

FIGURE 3. Thermal ellipsoid plot of the X-ray crystal structure of the cyclic peptide **2** at the 50% probability level with intramolecular H-bonds indicated. Apolar hydrogens have been omitted for clarity.

β-turn[52,53] together with residue 6 in its minor conformation (−72.56°, −7.39°). In contrast to the acyclic olefinic analogue, where residue 8 is in the α_R conformation,[28] the C-terminal residue in **1** adopts a left-handed polyproline II (P_{IIL}) conformation with $(\varphi, \psi) = (-57.83°, 159.12°)$. This fits well, however, into the empirical pattern found in a recent survey of nonhelical conformations of Aib residues in peptides. In a database of 143 crystal structures of Aib-containing helices with >3 residues with a C-terminal Aib, 86.5% of the C-terminal residues adopted the opposite helix sense than the rest of the molecule and 20.3% of these fell within the P_{IIL} region.[54]

The intramolecular H-bond lengths ($d_{C=O\cdots HN}$) vary between 2.115 Å (Aib1→Aib4) and 2.341 Å (Aib3→Aib6), with mean 2.193 Å and standard deviation 0.088 Å. These values are very similar to the ones found for the acyclic olefinic analogue (2.210 Å and 0.115 Å).[28] For both of these acyclic peptides the same pattern of H-bond length variations is observed. For both acyclic peptides, the longest H-bonds are between pairs of Aib residues on the N-terminal (residues 3 and 6) and on the C-terminal (residues 5 and 8) sides of the monosubstituted residues, respectively.

The carbonyl group of Aib7 forms an intermolecular H-bond to the carbamate NH of the Boc group, but there is no intermolecular peptide−peptide H-bond to the carbonyl of the methyl ester as is often seen in structures of Aib rich peptides.[54]

The cyclic peptide **2** ($C_{41}H_{69}N_{11}O_{12}$, $M_w = 908.05$) (Scheme 2) crystallized as colorless, plate-shaped crystals in space group $C2$, with unit cell parameters $a = 36.417(12)$, $b = 13.382(5)$, $c = 11.873(4)$ Å, $\alpha = 90.00°$, $\beta = 102.360(4)°$, $\gamma = 90.00°$ (monoclinic crystal system) and $Z = 4$. The X-ray structure was refined to a final R-factor of 0.039, which is unusually low for a molecule of this size.

Like the acyclic peptide **1** the cyclic octapeptide **2** forms a fully developed right handed 3_{10}-helix with all possible $i \rightarrow i+3$ intramolecular H-bonds present (Figure 3).

Whereas significant deviations from an ideal 3_{10}-helix with respect to individual dihedral angles were observed in the crystal structure of peptide **1**, the structure of peptide **2** represents a strikingly ideal 3_{10}-helix from residue 1−7. The average (φ, ψ)-angles are (−54.96°, −30.17°), deviating a mere 2.04° and 0.17° from ideality, making peptide **2** the most perfect cross-linked 3_{10}-helix to date (Table 1).

Importantly, the triazole bridge appears to strongly enforce a 3_{10}-helical conformation for residues 4, 6, and 7, effectively

(54) Aravinda, S.; Shamala, N.; Balaram, P. *Chem. Biodivers.* **2008**, *5*, 1238.

TABLE 1. Mean (φ, ψ)-Angles with Standard Deviations for the Cross-linked 3_{10}-Helical Peptides for Which Crystallographic Data Have Been Reported[a]

compound	φ	σ_φ	ψ	σ_ψ
ideal 3_{10}-helix	−57		−30	
1 (major)	−58.75	18.68	−27.93	16.34
1 (minor)	−64.22	15.61	−22.38	15.63
2	−54.96	6.79	−30.17	5.87
acyclic olefinic[28]	−62.32	15.23	−24.29	10.27
cyclic olefinic[28]	−68.35	24.04	−16.94	24.50
cyclic hydrogen[28]	−59.99	14.94	−27.52	15.59
acyclic api[29]	−54.20	4.35	−28.97	8.07
cyclic api (mol 1)[29]	−55.52	2.61	−26.78	6.11
cyclic api (mol 2)[29]	−54.94	3.83	−27.73	7.20

[a]The dihedral angles for residue 8 have been omitted for all peptides.

TABLE 2. Mean O···H Distances with Standard Deviations for the Intramolecular H-bonds in the Crystal Structures of 1 and 2[a]

compound	O···H	σ	O···H[b]	σ^b
1	2.193	0.088	2.164	0.056
2	2.118	0.075	2.102	0.071
2 (scaled)	2.087	0.084	2.058	0.051
acyclic olefinic[28]	2.210	0.115		
cyclic olefinic[28]	2.384	0.760	2.075	0.357
cyclic hydrogen[28]	2.335	0.195	2.257	0.034

[a]Positional parameters for amide H atoms were refined for **2** only. To facilitate comparison with **1**, scaled values are included for **2** after normalization of all N−H bonds to 0.880 Å (i.e., H atoms are moved along the covalent bond vectors so as to make the N−H distances equal to 0.880 Å, the fixed N−H distance used in the refinement of **1**). [b]The longest H-bond, i.e., between residues 4 and 7 for **2** and between 3 and 6 for **1** and the hydrocarbon stapled peptides, has been omitted.

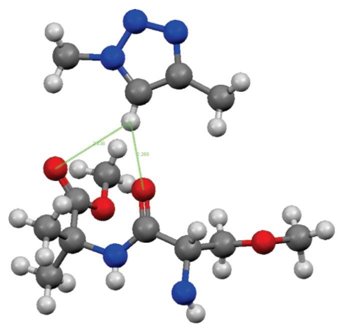

FIGURE 4. The triazole proton of one molecule forms a bifurcated nonclassical H-bond with residues 7 and 8 in another molecule. Only one of the two bifurcated H-bonds between two peptide molecules is shown. The remainder of the molecules has been omitted for clarity.

removing these as outliers in the Ramachandran plot (Figure 2). The deviations from ideality for these residues in peptide **2** are ($|\Delta\varphi|$, $|\Delta\psi|$) = (2.20°, 4.88°), (0.51°, 0.78°), and (10.93°, 9.25°), respectively, dramatically improved relative to **1**. This is opposite to the trend observed in the structures of the cyclic olefinic peptide and its hydrogenated analogue, where cyclization appeared to cause larger or unchanged deviations, with $(\varphi, \psi)_4$ = (−96.57°, 19.84°) and (−66.64°, −22.33°) and $(\varphi, \psi)_7$ = (−108.91°, 13.69°) and (−90.06°, 3.05°), respectively.[28] The sizes of the macrocycles and the rigid elements (triazole and carbon−carbon double bond) are important parameters that could be partially responsible for the different effects of the two staples on the backbone conformation. The macrocycle in **2** is slightly larger (19 atoms along the shortest path) than in the corresponding olefinic peptide (18 atoms). In addition, the rigid element in the CuAAC-derived bridge is also slightly larger than a carbon−carbon double bond.

The residues of the *p*-phenylene diacetic acid cross-linked Api/Aib peptide generally have close to ideal dihedral angles from residue 1 through to 7, but residue 4 (next to the first Api residue) has a slightly distorted ψ-angle (−22.69°), and the deviation from the ideal ψ-angle for residue 6 (−15.26°, $|\Delta\psi|$ = 14.74°) is larger than any φ/ψ-deviation from ideality for the first 7 residues of **2**.[29]

The C-terminal residue of **2** adopts an α_L conformation, in other words, the opposite helix sense as the rest of the molecule. This is statistically the most common conformation for a C-terminal Aib in Aib rich helices with >3 residues and is often due to head-to-tail intermolecular interactions with the Boc group in capped peptides or with solvent.[54] Interestingly, in the structure of **2** the dihedral angles of (46.80°, 49.93°) allow two peptide molecules to contact each other in a tail-to-tail fashion forming two bifurcated nonclassical C−H···O=C H-bonds between the triazole hydrogen and the carbonyl groups of residues 7 and 8 (Figure 4). This underlines a potential added advantage of a triazole in a helix stabilizing bridge, namely, its ability to make useful contacts to peptides/proteins. The triazole is approximately coplanar with the bifurcated H-bond. Interestingly, both of the Api peptides,[29] which also are highly 3_{10}-helical at residue 7, have C-terminal residues with conformations very similar to that of the C-terminal residue of **2**.

The overall similarity to an ideal 3_{10}-helix is also reflected in significantly shorter intramolecular H-bonds compared to **1** and the hydrocarbon stapled analogues (Table 2). The data for **1** refer to the structure with the alkyne side chain in its major orientation and the backbone in its major conformation (see Supporting Information for details).

As expected the longest H-bond observed in the structure of **2** is between residues 4 and 7 (2.232 Å, Δ_{2-1} = +0.103 Å), whose conformations change the most as they are pulled in toward more ideal 3_{10}-helical dihedral angles. However, all the remaining 5 intramolecular H-bonds are shorter in **2** than in **1**. The largest improvements are seen for Boc→Aib3 (Δ_{2-1} = −0.172 Å), Aib3→Aib6 (Δ_{2-1} = −0.193 Å) and Aib5→Aib8 (Δ_{2-1} = −0.184 Å). Interestingly, the Aib3→Aib6 H-bond is the one stretched the most in the cyclic hydrocarbon stapled peptides relative to their acyclic precursor ($\Delta_{cyclic-acyclic}$ = +0.386 Å and $\Delta_{cyclic-acyclic}$ = +1.585 Å) and is in fact broken in the cyclic olefinic peptide ($d_{O\cdots H}$ = 3.927 Å).[28]

NMR Spectroscopy. While the X-ray crystallographic studies provided atomic resolution detail of the conformations of **1** and **2** in the solid state, these may not be very representative of their solution phase structures. A careful investigation of the solution phase structures of **1** and **2** in the polar aprotic solvent CD_2Cl_2, including a detailed comparison with the corresponding crystal structures, was therefore undertaken using various NMR spectroscopic techniques.

The ^{1}H NMR spectra of **1** and **2** were found to be concentration dependent (Figure 5). In particular, the NH(Aib_1) ($\Delta\delta$ = 0.37 ppm) and NH(Aib_2) ($\Delta\delta$ = 0.20 ppm) resonances display remarkable downfield shifts when moving from a relatively dilute solution (9.9 mM) to a more concentrated solution (51 mM). The chemical shifts of the remaining protons, with the notable exception of one of the methyl groups, are much less concentration dependent

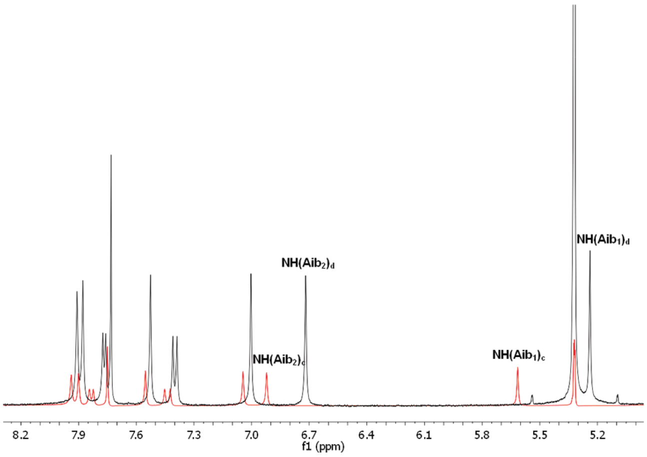

FIGURE 5. Overlay of the NH region of the ^{1}H NMR spectra of **2** in dilute (9.9 mM, 296 K, 400 MHz, black) and concentrated solution (51 mM, 298 K, 300 MHz, red). The NH(Aib$_1$) and NH(Aib$_2$) resonances are significantly downfield shifted in the more concentrated solution.

than $\delta_{NH(Aib1)}$ and $\delta_{NH(Aib2)}$. Remarkably, the concentration dependence of the ^{1}H NMR spectra, the selectivity of the effect on $\delta_{NH(Aib1)}$ and $\delta_{NH(Aib2)}$ and the magnitude and sign of the chemical shift changes may all be explained by invoking (concentration-independent) predominantly 3_{10}-helical backbone structures for **1** and **2** in CD_2Cl_2. It should be noted that NH(Aib$_1$) and NH(Aib$_2$) are the only amide NHs which do not participate in *intra*molecular H-bonding if the peptides adopt 3_{10}-helical structures (Figures 1 and 3) and the only NHs which thus may engage in *inter*molecular H-bonding without compromising the overall 3_{10}-helical structures of the peptides. We believe that the large and selective downfield shifts of $\delta_{NH(Aib1)}$ and $\delta_{NH(Aib2)}$ could be explained by hypothesizing that NH(Aib$_1$) and NH(Aib$_2$) form intermolecular H-bonds in concentrated CD_2Cl_2 solution, while the other NHs remain intramolecularly H-bonded. This would imply the presence of a monomer−dimer equilibrium, which could explain the concentration dependence of the ^{1}H NMR spectra.

The concentration dependence of the ^{1}H NMR spectra prompted the question of whether the structures in dilute solutions or in concentrated solutions are more similar to the crystal structures. The fact that NH(Aib$_1$) and NH(Aib$_2$) are not H-bonded to other peptide molecules in the crystal structures suggests that the structures in dilute solution are likely to be most similar to the solid state structures. It should be added that this concentration regime is also of greater biomedical relevance. The cyclic peptide **2** does form a dimer in the crystal, but this does not involve H-bonding to NH-(Aib$_1$) or NH(Aib$_2$) (Figure 4).

At any rate, caution is required when comparing solution phase structures in CD_2Cl_2 with the crystal structures, given the fact that the crystals were grown by slow evaporation of EtOAc (**1**) and (effectively) *i*PrOH solutions (**2**) rather than CD_2Cl_2 solutions.

To extract more detailed structural information 2D ROESY spectra were recorded in dilute CD_2Cl_2 solution (11 mM, 296 K, Figure 6 and Supporting Information). The 2D ROESY spectrum of **1** demonstrated the presence of 5 out of 7 possible NH(i)→NH(i+1) ROEs (the remaining two were not discernible, possibly due to overlap with the corresponding diagonal peaks) and the only possible C$^{\alpha}$H(i)→NH(i+2) ROE (Supporting Information), which are indicative of 3_{10}- or α-helical peptides.[55−57] However, the presence of the long-range C$^{\alpha}$H(i)→NH(i+3) ROE also typical of 3_{10}-helical peptides could not be established with certainty as the C$^{\alpha}$*H*-(azidonorVal) peak is overlapping with the C$^{\alpha}$H(propSer)-C*H*$_2$O peak, which has an ROE to N*H*(propSer) (Supporting Information).

Gratifyingly, ROEs characteristic of a 3_{10}-helical structure was also found in the 2D ROESY spectrum of **2**, including all possible short-range NH(i)→NH(i+1), medium range C$^{\alpha}$H(i)→NH(i+2), and long-range C$^{\alpha}$H(i)→NH(i+3) ROEs (Figure 6).

A commonly used upper distance constraint for a weak ROE is on the order of 5.0 Å.[58] In order to determine more precisely the extent to which the solution structures of **1** and **2** mimic their corresponding crystal structures, all proton pairs closer than 5.0 Å in the crystal structures, which should give rise to ROEs if the crystal structure is preserved in solution, were identified. In the case of **1** the distance measurements were performed on the structure with the alkyne side chain and backbone at Aib6 in their major conformations. A careful analysis of the experimental 2D ROESY spectra recorded in dilute CD_2Cl_2 solution for the presence or absence of these ROEs was undertaken. The results are summarized in Figure 7.

For **1** the general correlation between the predictions based on the crystal structure and the experimental solution phase spectrum is quite good, with 18 (45%) predicted ROEs present and 11 (27.5%) absent. However, the presence/absence of an additional 11 (27.5%) ROEs could not unambiguously be decided because of overlap with other peaks. Importantly, the correlation appears to be even better for the cyclic peptide **2**, with 27 (63%) predicted ROEs present in the experimental spectrum, only 3 (7%) undecidable, and 13 (30%) absent. For both compounds it should be added that a large fraction of the correlations that were not found experimentally corresponds to distances between 4.0 and 5.0 Å in the crystal structure and are expected to be weak and potentially difficult to distinguish from background noise in dilute solutions.

An examination of the individual *backbone-to-backbone* ROEs reveals the presence of all possible NH(i)→NH(i+1) ROEs, but none of the predicted NH(i)→NH(i+2) ROEs. However, the latter finding should not be considered as strong evidence against a 3_{10}-helical structure, as the NH(i)→NH(i+2) distance is approximately 4.5 Å in a 3_{10}-helix, giving rise to a weak ROE at best, but can be much shorter in nonhelical peptides, as can be appreciated from a molecular model. When it comes to the predicted C$^{\alpha}$H→NH type ROEs the accordance between theory and experiment is very good for both peptides.

Some of the *side chain-to-backbone* ROEs, i.e., side chain-to-NH and side chain-to-C$^{\alpha}$H ROEs, are quite informative, as their presence/absence appear to be particularly sensitive to small changes in backbone structure away from the

(55) Rai, R.; Aravinda, S.; Kanagarajadurai, K.; Raghothama, S.; Shamala, N.; Balaram, P. *J. Am. Chem. Soc.* **2006**, *128*, 7916.
(56) Williams, D. H.; Fleming, I. *Spectroscopic Methods in Organic Chemistry*, 5th ed.; McGraw-Hill: New York, 1995; pp 140.
(57) Wüthrich, K. *NMR of Proteins and Nucleic Acids*; John Wiley & Sons: New York, 1986.
(58) Ma, M. T.; Hoang, H. N.; Scully, C. C. G.; Appleton, T. G.; Fairlie, D. P. *J. Am. Chem. Soc.* **2009**, *131*, 4505.

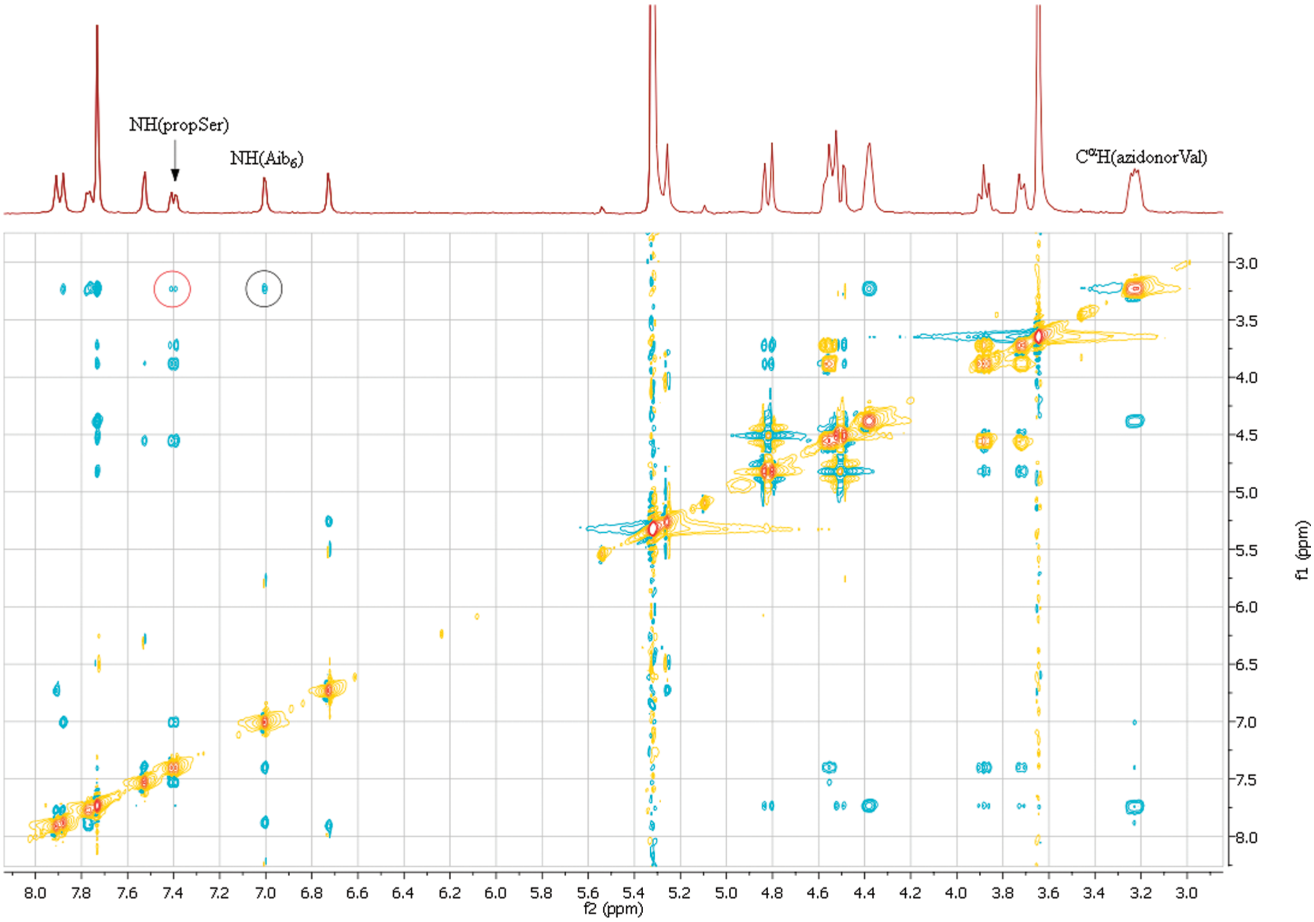

FIGURE 6. Partial 2D ROESY spectrum of **2** displaying the only possible medium range $C^{\alpha}H(i) \rightarrow NH(i+2)$ (black circle) and long-range $C^{\alpha}H(i) \rightarrow NH(i+3)$ ROE (red circle). Note that not all ROEs referred to in Figure 7 are visible at the chosen spectrum intensity.

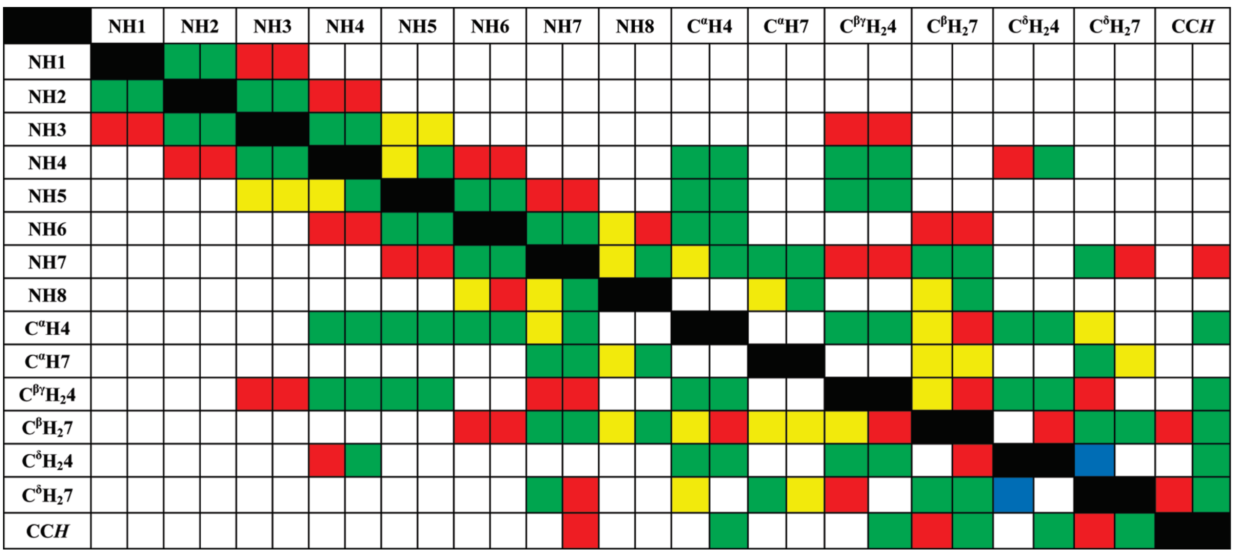

FIGURE 7. ROEs observed in the 2D ROESY spectra of **1** and **2** in dilute CD_2Cl_2 solution and comparison of the solution structures of **1** and **2** in CD_2Cl_2 with their respective crystal structures. Color code: Green signifies an ROE that should be observed if the crystal structure is preserved in solution and *is found* experimentally. Yellow signifies an ROE that should be observed if the crystal structure is preserved in solution, but cannot unambiguously be identified experimentally because of overlap with other ROEs, artifact peaks (e.g., TOCSY peaks), or diagonal peaks under the given experimental conditions. Red signifies an ROE that should be observed if the crystal structure is preserved in solution, but is *not found* in the experimental spectra or could not be distinguished from background noise. White fields correspond to distances greater than 5.0 Å in the crystal structure. Blue signifies the presence of a correlation in the experimental spectrum that was not predicted by the crystal structure. *For each correlation the left-hand columns refer to peptide **1** and the right-hand columns to peptide **2**.* Note that CCH is the alkyne proton in **1** and the triazole proton in **2**. All methyl groups and the Boc group have been omitted.

3_{10}-helical crystal structures. This is especially the case for the $C^{\delta}H_2(i) \rightarrow NH(i)$ interactions in the acyclic peptide **1**, and to a lesser degree the $C^{\beta}H_2(i) \rightarrow NH(i)$ interactions. In the 3_{10}-helical crystal structure the torsional angle $C^{\beta}-C^{\alpha}-N-H$ is small and positions the NH proton and the side chain on the same side of the backbone with close to minimal distance separation. The distance $C^{\delta}H_2(4) \rightarrow NH(4)$ is 4.20 Å in the crystal structure, making this a quite sensitive test for local helical structure. The absence of an observable $C^{\delta}H_2(4) \rightarrow NH(4)$ correlation for **1** could indicate that the peptide backbone enjoys substantial conformational freedom, at least locally. The $C^{\delta}H_2(4) \rightarrow NH(4)$ ROE is present in the 2D ROESY spectrum of **2**, for which the corresponding crystal structure distance is 4.87 Å. This is an important difference between the two compounds. The $C^{\delta}H_2(7) \rightarrow NH(7)$ correlation (3.56 Å in the crystal structure) is, however, present in **1**. The shorter distance compared with $C^{\delta}H_2(4) \rightarrow NH(4)$ (4.20 Å) suggests that it is less sensitive to backbone changes away from the crystal structure than the $C^{\delta}H_2(4) \rightarrow NH(4)$ ROE. In contrast to **1**, the $C^{\delta}H_2(7) \rightarrow NH(7)$ is absent from the 2D ROESY spectrum of the cyclic peptide **2**, but this does not necessarily imply a large deviation from the crystal structure, as the crystal structure distance is 4.69 Å, placing it close to the detection limit already in a perfect 3_{10}-helix.

There are no observable differences between **1** and **2** regarding the presence/absence of $C^{\beta}H_2 \rightarrow NH$ type ROEs. The presence of $C^{\beta}H_2(i) \rightarrow NH(i)$ interactions in both peptides should be noted in support of a predominantly 3_{10}-helical backbone structure. However, larger backbone conformational changes are required to completely abolish these than is the case for the $C^{\delta}H_2(i) \rightarrow NH(i)$ ROEs discussed earlier. The absence of predicted $NH(i) \rightarrow C^{\beta}H_2(i+1)$ and presence of $C^{\beta}H_2(i) \rightarrow NH(i+1)$ correlations in both peptides are less informative.

The absence of $C^{\alpha}H(4) \rightarrow C^{\beta}H_2(7)$ interactions in the cyclic peptide **2** is a bit surprising (distance 4.21 Å in the crystal). For the acyclic peptide **1** the presence or absence of this ROE cannot be decided.

Side chain-to-side chain correlations may also be informative, especially for the acyclic peptide, for which the side chains of residues 4 and 7 are likely to be too far apart to give rise to observable ROEs in many nonhelical conformations. Most of these are absent in both peptides, including the expected $C^{\beta\gamma}H_2(4) \rightarrow C^{\beta}H_2(7)$ and $C^{\delta}H_2(4) \rightarrow C^{\beta}H_2(7)$ ROEs for **2** and the $C^{\beta\gamma}H_2(4) \rightarrow C^{\delta}H_2(7)$ ROE for **1**.

Finally, a very weak ROE that was not predicted on the basis of the X-ray structure was observed between $C^{\delta}H_2(4)$ and $C^{\delta}H_2(7)$ for **1**. In general, the absence of many extra peaks not predicted by the crystal structure provides further evidence that the solution structure closely mimics the crystal structure. However, the presence of the unexpected $C^{\delta}H_2(4) \rightarrow C^{\delta}H_2(7)$ ROE may nevertheless be taken as evidence in favor of a 3_{10}-helical structure, because it means that the side chains of residues 4 and 7 are on the same side of the molecule, which is what one would expect for a 3_{10}-helical peptide.

As a final note, the 2D ROESY spectra display ROEs characteristic of 3_{10}-helices independently of concentration. Hence, the possible presence of a monomer–dimer equilibrium is not expected to constitute a major complication for the structural analysis of **1** and **2** in solution.

The signal dispersion of the methyl resonances is significantly greater for **2** than for **1** (Figure 8). This indicates a smaller degree of conformational mobility/averaging on the NMR time scale in the former case and thus provides evidence for a more stable 3_{10}-helix.

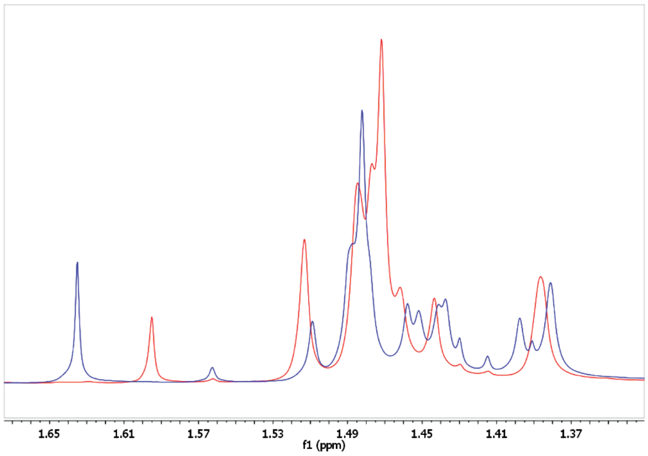

FIGURE 8. Methyl resonances in the ^1H NMR spectra of **1** (red) and **2** (blue) (c_1 = 10 mM, c_2 = 9.9 mM, T_1 = 295 K, T_2 = 296 K). The greater dispersion of the resonances for the cyclic peptide may be taken as evidence for a more structured peptide in solution (less conformational averaging).

TABLE 3. Chemical Shifts of NH Resonances in Dilute (c_1 = 10 mM, c_2 = 9.9 mM, T_1 = 295 K, T_2 = 296 K) CD_2Cl_2 Solution

residue	$\delta_{acyclic}$	δ_{cyclic}	$\Delta\delta$
Aib1	5.21	5.24	+0.03
Aib2	6.69	6.72	+0.03
Aib3	7.92	7.91	−0.01
azidonorVal	7.80	7.77	−0.03
Aib5	7.84	7.88	+0.04
Aib6	7.29	7.00	−0.29
propSer	7.55	7.40	−0.15
Aib8	7.56	7.53	−0.03

The chemical shifts of the NH resonances of the cyclic peptide **2** are generally very similar to those of **1** (Table 3) and demonstrate that the H-bond lengths and angles of the two peptides most likely are relatively similar in CD_2Cl_2 solution. The only exceptions are $NH(Aib_6)$ and NH(propSer), which are shifted 0.29 and 0.15 ppm upfield for **2**. The 1D and 2D NMR data taken together demonstrate that $i \rightarrow i+3$ side chain-to-side chain macrocyclization by CuAAC results in a close-to-ideal and conformationally stable 3_{10}-helical peptide.

Measurement and Simulation of 2D IR Spectra. Conventional linear IR response of the amide-I mode is widely used to obtain structural information of polypeptides.[59] Going beyond 1D, 2D IR spectroscopy measures nonlinear response of the mode, which has higher sensitivity to the underlying biomolecular structure.[60−62] In this study we measured FT IR and 2D IR spectra of **1** and **2** in CH_2Cl_2 to obtain insights into the backbone conformation of these peptides in a polar aprotic solvent. Also, the spectral profiles were simulated based on crystal structures established by the X-ray diffraction analysis. Details of our 2D IR spectrometer, data collection, and calculation protocol have been described previously.[46,63,64]

(59) Krimm, S.; Bandekar, J. *Adv. Protein Chem.* **1986**, *38*, 181.
(60) Zhuang, W.; Hayashi, T.; Mukamel, S. *Angew. Chem., Int. Ed.* **2009**, *48*, 3750.
(61) Kim, Y. S.; Hochstrasser, R. M. *J. Phys. Chem. B* **2009**, *113*, 8231.
(62) Hunt, N. T. *Chem. Soc. Rev.* **2009**, *38*, 1837.

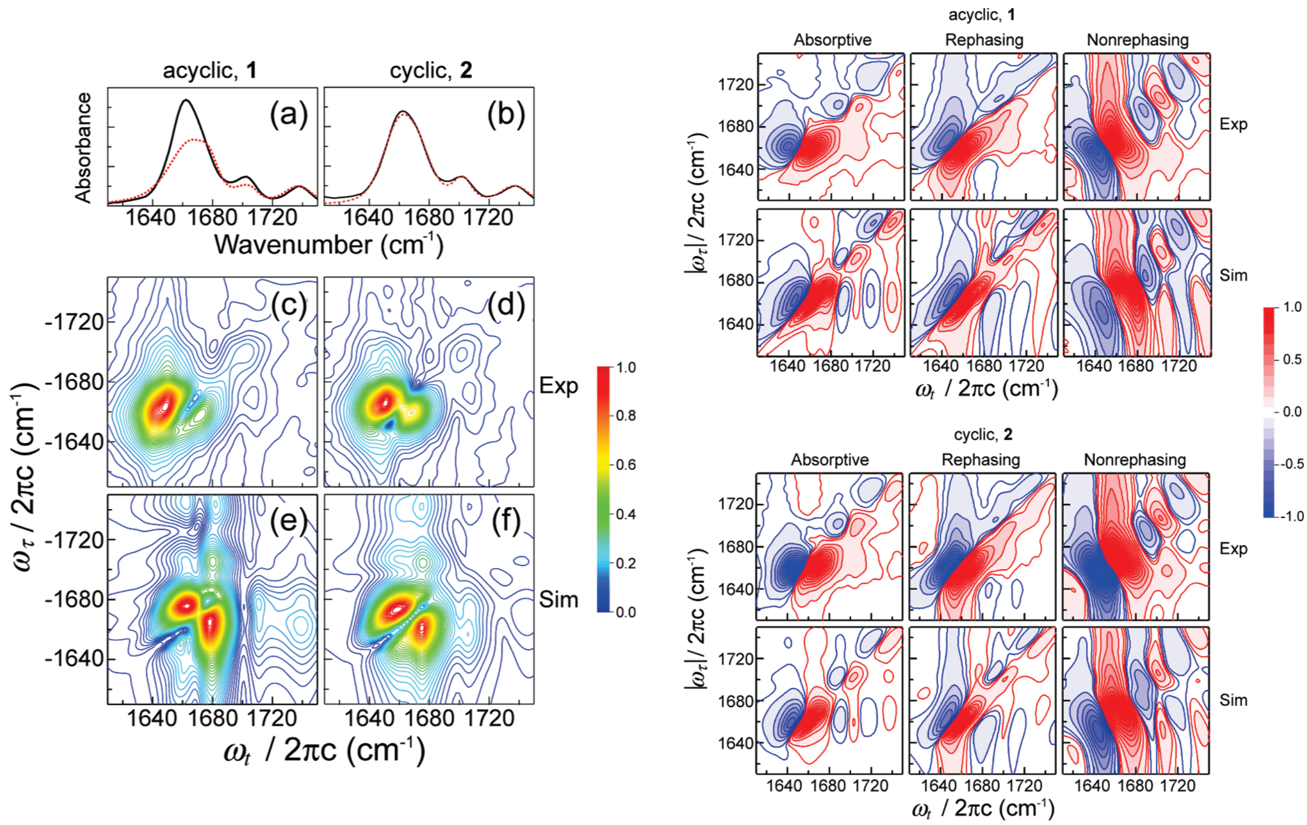

FIGURE 9. (a, b) Measured (black solid) and simulated (red dashed) linear IR spectra for **1** and **2**. (c, d) 2D IR cross-peak patterns in CH_2Cl_2 observed under the double-crossed polarization configuration. (e, f) Simulated cross-peak patterns based on the peptide backbone conformations of **1** and **2** in the crystal state. Shown on the right are the measured and simulated absorptive and the real parts of the rephasing and nonrephasing 2D IR spectra under the perpendicular polarization configuration.

The specifics relevant to the data discussed below are given in the Supporting Information.

The top panels in Figure 9a and b show the measured FT IR spectra (black solid) of **1** and **2**, respectively, in CH_2Cl_2 (~6 mM, a thickness of 180 μm). The spectra were normalized by the peak absorbance of the methyl ester C═O band at 1738 cm^{-1} after subtracting the solvent spectrum. We assign the small band at 1701 cm^{-1} to the urethane C═O of the N-terminus Boc group and the broad band at 1662 cm^{-1} to the amide-I modes. The line shapes of the amide-I bands of the two peptides are slightly different, more rounded at the peak for **2** but pointy for **1**. The full-width-half-maximum are 27.7 and 30.8 cm^{-1}, respectively. It is not straightforward, however, to infer from the linear spectra whether **1** and **2** in CH_2Cl_2 maintain the same 3_{10}-helical conformation as observed in the crystal states, or if their structures have changed to other conformations, such as α-helix and P_{IIL}.

The absorptive and the real parts of rephasing and nonrephasing 2D IR spectra of **1** and **2** measured under the ⟨*Y*, *Y*, *Z*, *Z*⟩ polarization configuration are shown on the right in Figure 9. The three positive peaks along the diagonal line of the absorptive spectrum correspond to the 0−1 transitions, whereas the three negative peaks are the 1−2 transitions, which are anharmonically shifted from the 0−1 in the ω_t direction. For the rephasing and nonrephasing spectra, the nodal lines between the 0−1 and 1−2 transitions are parallel and perpendicular to the diagonal, respectively. These 2D IR spectra look almost indistinguishable between **1** and **2**.

The amide-I 2D IR cross-peak pattern obtained under the double-crossed polarization can much more sensitively distinguish subtle structural differences, for example, between 3_{10}- and α-helices.[63,64] In general, the experimental and simulated 2D profile exhibits a doublet pattern for the former and a multiple-peak pattern for the latter.[64,65] Figure 9c and d presents the absolute magnitude cross-peak patterns of **1** and **2**, respectively. A doublet clearly shows up in the amide-I region. Weak cross-peaks between the amide-I and the urethane C═O modes are also observed. The doublet pattern of **1** is similar to that of **2**, but some subtle differences can also be noticed. For **2**, the line shape and relative intensity of the lower diagonal peak to the upper peak (0.68) are very close to those observed for other 3_{10}-helical peptides with Aib and (αMe)Val residues.[63,64] For **1**, the two peaks in the doublet are more elongated along the diagonal, merged into each other at a lower frequency, and their intensity ratio is 0.45. This result suggests that **1** and **2** are both 3_{10}-helical in the solution but their structures are slightly different. It is conceivable that **1** may be more disordered than **2** because it lacks the side chain-to-side chain CuAAC constraint. Our previous theoretical study shows that the rephasing cross-peak pattern differs from a doublet with the appearance

(63) Maekawa, H.; Toniolo, C.; Broxterman, Q. B.; Ge, N.-H. *J. Phys. Chem. B* **2007**, *111*, 3222.
(64) Maekawa, H.; Toniolo, C.; Moretto, A.; Broxterman, Q. B.; Ge, N.-H. *J. Phys. Chem. B* **2006**, *110*, 5834.
(65) Sengupta, N.; Maekawa, H.; Zhuang, W.; Toniolo, C.; Mukamel, S.; Tobias, D. J.; Ge, N.-H. *J. Phys. Chem. B* **2009**, *113*, 12037.

of extra features as the peptide conformation increasingly deviates from an ideal 3_{10}-helix.[65] The absence of extra features suggests that the structural difference between **1** and **2** is small in CH_2Cl_2 despite the quite different dihedral angles of the residues 4, 6, and 7 observed in the crystal state.

To further address these points, we performed model calculations to examine how similar or different the 2D IR spectral patterns would be if the crystal structures are preserved in solution. Figure 9e and f presents the simulated 2D IR cross-peak pattern using an ensemble of peptide structures with the backbone dihedral angles in Gaussian distributions centered at the crystal structures of **1** and **2**, respectively. The simulated 2D IR pattern of **2** shows a clear amide-I doublet along with some cross-peaks between the amide-I and the capping C=Os. The linear IR spectrum (Figure 9b, red dashed) and 2D absorptive and the real parts of the rephasing and nonrephasing spectra (Figure 9, bottom panels on the right) were also calculated using the same parameters, and the agreement with the experimental spectrum is quite good. This suggests that the solution structure of **2** is close to that of an ideal 3_{10}-helix. In contrast, the crystal structure of **1** gave rise to quite different linear and 2D IR spectra from those of **2**. The calculated linear spectrum of the major backbone conformer consists of two overlapping, broad amide-I bands with the lower frequency band having a stronger peak intensity. The linear spectrum of the minor backbone conformer also exhibits two bands with an opposite trend in the peak intensity. The population weighted spectrum (Figure 9a) shows hints of overlapping features. The cross-peak pattern in Figure 9e exhibits a more spread doublet with additional shoulders than that characteristic of an ideal 3_{10}-helix. Note that the simulated cross-peak pattern is still different from the ideal α-helix conformation [(ϕ, ψ) = (−63°, −42°)] we obtained previously.[63,64] Also, the calculated 2D absorptive spectrum of **1** is more elongated along the diagonal than that of **2**. The experimental and simulation results indicate that the different backbone conformations of **1** and **2** in the crystal state are no longer preserved in CH_2Cl_2.

The results from our linear and 2D IR experiments and simulations are consistent with the findings from 1D and 2D NMR measurements. Both peptides remain 3_{10}-helical in solution. Comparing to **2**, the solution structure of the acyclic peptide **1** is more flexible and/or disordered. It also exhibits larger deviations from the crystal structure. The difference in their behavior can be attributed to the effect of the side chain-to-side chain constraint on peptide conformation.

Conclusion

In summary, the feasibility of side chain-to-side chain cross-linking by CuAAC in a 3_{10}-helical Aib rich peptide has been demonstrated. An attractive feature of the cyclic product **2** is its significantly higher aqueous solubility (> 1 mM) compared to **1**. 2D IR and 2D ROESY experiments confirmed that the cyclic peptide **2** retains a 3_{10}-helical structure in the polar aprotic solvent CD_2Cl_2. The first X-ray crystallographic investigation of a helical peptide with a triazole derived cross-link has revealed that **2** is the most perfect cross-linked 3_{10}-helical peptide so far studied in the crystal state, with mean (φ, ψ)-angles deviating less than 2° from ideality.

The closeness to ideality of the conformational angles in the solid state strongly suggests that the CuAAC side chain-to-side chain cross-linking methodology may have significant utility applied to peptides and peptidomimetics of interest in chemical biology and biomedicine, in particular to synthetic analogues of the Pro138-Gly144 segment of human AQP4.[20]

Experimental Section

Full experimental details for the crystallization of **1** and **2**, acquisition of NMR, FT IR and 2D IR data, model calculations of linear and 2D IR spectra and syntheses of intermediates may be found in the available Supporting Information. The crystal structures of **1** and **2** have been deposited at the Cambridge Crystallographic Data Centre (accession codes CCDC 770131 and CCDC 770132).

***N-tert*-Butoxycarbonyl α,α-Dimethylglycyl α,α-Dimethylglycyl α,α-Dimethylglycyl *δ*-azido-L-norvalyl α,α-Dimethylglycyl α,α-Dimethylglycyl *O*-Propynyl-L-seryl α,α-Dimethylglycyl Methyl Ester 1.** *δ*-Azido-L-norvalyl α,α-dimethylglycyl α,α-dimethylglycyl *O*-propynyl-L-seryl α,α-dimethylglycyl methyl ester trifluoroacetate **4** (0.551 g, 0.827 mmol) and *N-tert*-butoxycarbonyl α,α-dimethylglycyl α,α-dimethylglycyl α,α-dimethylglycine[28] (0.309 g, 0.827 mmol) (see Supporting Information for details on preparation) were suspended in CH_2Cl_2 (5 mL), and a solution of *N*,*N*-diisopropylethylamine (0.107 g, 0.828 mmol) in CH_2Cl_2 (7 mL) added. HOBt hydrate (0.127 g, 0.829 mmol) and then EDC hydrochloride (0.174 g, 0.908 mmol) were added together with more CH_2Cl_2 (5 mL) at room temperature. The reaction mixture was stirred for 45 h at room temperature before being diluted with CH_2Cl_2 (65 mL). The solution was washed with 5% (w/w) citric acid monohydrate solution (3 × 35 mL), 7.5% (w/w) K_2CO_3 solution (3 × 35 mL), and saturated brine (35 mL). The solution was dried with anhydrous $MgSO_4$ and the solvent was evaporated affording a white solid (0.595 g). The solid (0.573 g) was purified by flash column chromatography (eluent CH_2Cl_2/acetone (3:1)) affording the title compound as a white solid (0.323 g, 43%): ^{1}H NMR (400 MHz, CD_2Cl_2, 10 mM, 295 K) δ 7.92 (s, 1H, N*H*(Aib$_3$)), 7.84 (s, 1H, N*H*(Aib$_5$)), 7.80 (d, *J* = 5.1 Hz, 1H, N*H*(azidonorVal)), 7.56 (s, 1H, N*H*(Aib$_8$)), 7.55 (d, *J* = 8.0 Hz, 1H, N*H*(propSer)), 7.29 (s, 1H, N*H*(Aib$_6$)), 6.69 (s, 1H, N*H*(Aib$_2$)), 5.21 (s, 1H, N*H*(Aib$_1$)), 4.44 (td, *J* = 8.3, 3.5 Hz, 1H, C$^\alpha$*H*(propSer)), 4.23 (dd, *J* = 15.6, 2.4 Hz, 1H, C*H*HCCH), 4.18 (dd, *J* = 16.0, 2.4 Hz, 1H, CH*H*CCH), 3.97−3.80 (m, 3H, C$^\alpha$*H*(azidonorVal)/C*H*$_2$O), 3.65 (s, 3H, OC*H*$_3$), 3.33 (t, *J* = 6.8 Hz, 2H, C*H*$_2$N$_3$), 2.48 (t, *J* = 2.3 Hz, 1H, CC*H*), 2.02−1.62 (m, 4H, C*H*$_2$C*H*$_2$CH$_2$N$_3$), 1.61−1.36 (m, 45H, C*H*$_3$/(C*H*$_3$)$_3$); ^{13}C NMR (75 MHz, CD_2Cl_2, 8.1 mM, 298 K) δ 177.2, 176.1, 175.5, 175.5, 175.4, 175.2, 173.9, 170.0, 156.2, 82.1, 80.7, 74.6, 70.0, 58.8, 57.5, 57.4, 57.4, 57.4, 57.1, 57.0, 56.3, 54.7, 52.4, 51.8, 28.5, 28.5, 28.0, 28.0, 27.7, 27.5, 27.4, 26.5, 25.5, 25.2, 23.8, 23.5, 23.3, 23.3, 23.1; HRMS (*m*/*z*) [M + Na]$^+$ calcd for $C_{41}H_{69}N_{11}O_{12}$Na, 930.5024, found 930.5017. Anal. Calcd for $C_{41}H_{69}N_{11}O_{12}$: C, 54.23; H, 7.66; N, 16.97. Found: C, 54.2; H, 7.6; N, 16.6.

Methyl 2-Methyl-2-((5S,14S)-8,8,11,11-tetramethyl-5-(2,2,6,6,9,9,12,12-octamethyl-4,7,10-trioxo-3-oxa-5,8,11-triazatridecanamido)-6,9,12-trioxo-16-oxa-1,7,10,13,19,20-hexaazabicyclo[16.2.1] henicosa-18(21),19-dienecarboxamido)propanoate 2. (5*S*,14*S*)-14-(1-Methoxy-2-methyl-1-oxopropan-2-ylcarbamoyl)-8,8,11,11-tetramethyl-6,9,12-trioxo-16-oxa-1,7,10,13,19,20-hexaazabicyclo[16.2.1]henicosa-18(21),19-dien-5-aminium 2,2,2-trifluoroacetate **6** (0.332 g, 0.498 mmol) and *N-tert*-butoxycarbonyl α,α-dimethylglycyl α,α-dimethylglycyl α,α-dimethylglycine[28] (0.186 g, 0.498 mmol) (see Supporting Information for details on preparation) were suspended in CH_2Cl_2 (3 mL) and a solution of *N*,*N*-diisopropylethylamine (0.065 g, 0.50 mmol) in CH_2Cl_2 (4 mL) was added. HOBt hydrate (0.076 g, 0.50 mmol) and then EDC hydrochloride (0.105 g, 0.548 mmol) were added at room temperature together with additional CH_2Cl_2 (3 mL). The reaction mixture was stirred for 44 h at room temperature before being diluted with CH_2Cl_2 (40 mL). The solution was washed with

5% (w/w) citric acid monohydrate solution (3 × 20 mL), 7.5% (w/w) K_2CO_3 solution (3 × 20 mL), and saturated brine (20 mL). The solution was dried with anhydrous $MgSO_4$, and the solvent was evaporated affording the title compound as a white solid (0.331 g, 73%): ^{1}H NMR (400 MHz, CD_2Cl_2, 9.9 mM, 296 K) δ 7.91 (s, 1H, N*H*(Aib_3)), 7.88 (s, 1H, N*H*(Aib_5)), 7.77 (d, J = 6.0 Hz, 1H, N*H*(azidonorVal)), 7.73 (s, 1H, C_2HN_3), 7.53 (s, 1H, N*H*(Aib_8)), 7.40 (d, J = 8.4 Hz, 1H, N*H*(propSer)), 7.00 (s, 1H, N*H*(Aib_6)), 6.72 (s, 1H, N*H*(Aib_2)), 5.24 (s, 1H, N*H*(Aib_1)), 4.82 (d, J = 13.0 Hz, 1H, OC*H*HC_2HN_3), 4.55 (td, J = 8.4, 2.8 Hz, 1H, $C^\alpha H$(propSer)), 4.51 (d, J = 13.2 Hz, 1H, OCH*H*C_2HN_3), 4.38 (t, J = 5.7 Hz, 2H, $CH_2N_3C_2H$), 3.88 (t, J = 8.5 Hz, 1H, C^αHC*H*HO), 3.72 (dd, J = 9.0, 2.9 Hz, 1H, C^αHCH*H*O), 3.65 (s, 3H, OCH_3), 3.23 (ddd, J = 11.7, 5.9, 3.8 Hz, 1H, $C^\alpha H$(azidonorVal)), 2.31−2.17 (m, 1H, CH_2-C*H*HCH_2), 2.07−1.93 (m, 2H, C^αHC*H*HCH_2CH_2/CH_2CH*H*-CH_2), 1.79−1.68 (m, 1H, C^αHCH*H*CH_2CH_2), 1.64 (s, 3H, CH_3), 1.58−1.35 (m, 42H, $CH_3/(CH_3)_3$); ^{13}C NMR (75 MHz, CD_2Cl_2, 51 mM, 298 K) δ 177.4, 175.9, 175.8, 175.6, 175.6, 175.5, 173.7, 170.0, 156.4, 145.3, 125.2, 81.9, 70.0, 65.3, 57.6, 57.5, 57.4, 57.3, 57.1, 56.4, 55.2, 54.4, 52.5, 49.7, 28.6, 28.3, 27.9, 27.9, 27.3, 27.2, 27.0, 25.4, 25.3, 24.8, 23.7, 23.4, 23.3, 23.2, 23.0; HRMS (m/z) $[M + H]^+$ calcd for $C_{41}H_{70}N_{11}O_{12}$, 908.5205, found 908.5194. Anal. Calcd for $C_{41}H_{69}N_{11}O_{12}$: C, 54.23; H, 7.66; N, 16.97. Found: C, 54.0; H, 7.6; N, 16.5.

Acknowledgment. Ø.J., C.H.G., P.R., O.P.O., M.A.-M., and J.K. gratefully acknowledge Inven2 AS, the Technology Transfer Office of the University of Oslo, and the Norwegian Research Council for financial support through a verification grant and professor Frode Rise (University of Oslo) and Göran Schömer (Bruker Biospin Scandinavia) for NMR technical support. H.M. and N.-H.G. gratefully acknowledge grant support from the US National Science Foundation (CHE-0802913).

Supporting Information Available: Synthesis schemes, full experimental details for syntheses, compound characterization data, crystallization conditions, crystallographic data in CIF format, experimental details for acquisition of X-ray, NMR, linear IR and 2D IR data, model calculations of linear and 2D IR spectra, Ramachandran plots, and partial 2D ROESY spectra. This material is available free of charge via the Internet at http://pubs.acs.org.